

Article

Effect of Pulse Laser Welding Parameters and Filler Metal on Microstructure and Mechanical Properties of Al-4.7Mg-0.32Mn-0.21Sc-0.1Zr Alloy

Irina Loginova *, Asmaa Khalil , Andrey Pozdniakov, Alexey Solonin and Vadim Zolotarevskiy

Department of Physical Metallurgy of Non-Ferrous Metals, National University of Science and Technology MISiS, Moscow 119049, Russia; eng.asmaa.m.khlil@outlook.com (A.K.); pozdniakov@misis.ru (A.P.); solonin@misis.ru (A.S.); zolotor@misis.ru (V.Z.)

* Correspondence: i-popkova@list.ru; Tel.: +7-916-659-35-37

Received: 13 November 2017; Accepted: 12 December 2017; Published: 14 December 2017

Abstract: The effect of pulse laser welding parameters and filler metal on microstructure and mechanical properties of the new heat-treatable, weldable, cryogenic Al-4.7Mg-0.32Mn-0.21Sc-0.1Zr alloy were investigated. The optimum parameters of pulsed laser welding were found. They were 330–340 V in voltage, 0.2–0.25 mm in pulse overlap with 12 ms duration, and 2 mm/s speed and ramp-down pulse shape. Pulsed laser welding without and with Al-5Mg filler metal led to the formation of duplex (columnar and fine grains) as-cast structures with hot cracks and gas porosity as defects in the weld zone. Using Al-5Ti-1B filler metal for welding led to the formation of the fine grain structure with an average grain size of $4 \pm 0.2 \mu\text{m}$ and without any weld defects. The average concentration of Mg is 2.8%; Mn, 0.2%; Zr, 0.1%; Sc, 0.15%; and Ti, 2.1% were formed in the weld. The ultimate tensile strength (UTS) of the welded alloy with AlTiB was 260 MPa, which was equal to the base metal in the as-cast condition. The UTS was increased by 60 MPa after annealing at 370 °C for 6 h that was 85% of UTS of the base alloy.

Keywords: aluminum alloys; electron microscopy; stress/strain measurements; laser methods; grains and interfaces

1. Introduction

Al-Mg alloys with scandium additives have been actively developed and are already used in industry. Scandium greatly increases the yield stress (YS) of such alloys and, ultimately, their strength due to the formation of the Al₃Sc nanoparticle phase, which retains the semi-finished deformed structure, even after annealing at temperatures above 300 °C [1–3].

Al-Mg alloys are the weldable aluminum alloys. However they have high hot cracking susceptibility during argon-arc welding and high gas porosity after gas welding [4,5]. Hot cracking susceptibility depends on the value of the effective solidification range (ESR), the strength, and the plasticity in this range [6–8]. The maximum ESR and hot cracking susceptibility for Al-Mg alloys is indicated at 0.8% Mg [6–8]. Increasing the magnesium content to more than 6% significantly decreased the formation of hot cracks [6–8]. Another way of decreasing hot cracking is grain refining. For example, the alloying of Al alloys by small additives of Ti was found to decline sharply the hot cracking index [6]. The role of the inclusions and segregation is not unique. On the one hand, the hot cracking decreased if the inclusions and segregation is the effective refiners. On the other hand, the inclusions and segregation are the internal stress concentrators and, in this case, the hot cracking susceptibility increased.

The ultimate tensile strength (UTS) of the weld for Al-5Mg was 250–260 MPa argon-arc welding and for Al-7Mg (270–280 MPa) after gas welding [9]. High hot cracking susceptibility and gas porosity

can be decreased by laser welding or friction stir welding [3]. Studies [10,11] have reported that the UTS of the friction stir welded Al-4Mg with Sc and Zr additives was 320 MPa. However microstructure of the weld was asymmetric with inhomogeneous hardness. The formation of the fine grain structure, dispersive Al_3Er phase, and low Mg evaporation increased UTS of laser-welded Al-4.7Mg-0.7Mn-0.3Er alloy up to 320 MPa. Al-4.7Mg-0.62Mn and Al-4.5Mg-0.57Mn-0.32Er-0.14Zr alloys were laser welded in [12]. The UTS was 290 and 300 MPa, respectively. Er and Zr additives led to the formation of the $\text{Al}_3(\text{Er,Zr})$ dispersoids and an increase in UTS. However, Fu and others [13] have studied the thermodynamic stability of the $\text{Al}_3(\text{Sc}_{1-x}\text{Zr}_x)$ and $\text{Al}_3(\text{Er}_{1-x}\text{Zr}_x)$ particles that were formed after gas tungsten arc welded joints of the Al-Mg alloy. It was concluded that $\text{Al}_3(\text{Sc}_{1-x}\text{Zr}_x)$ particles have higher thermodynamic stability than $\text{Al}_3(\text{Er}_{1-x}\text{Zr}_x)$ particles. The ultimate strength and yield strength of Al-Mg-Sc joint were 338 MPa and 238 MPa, respectively; the ultimate strength and yield strength of Al-Mg-Er welded joints were 320 MPa and 183 MPa, respectively.

A new alternative rapid and economical method to obtain joints of different metals and alloys is friction drilling [14–16]. This is based on the material flow, by using the heat caused by the friction of a conical shape rotary tool without cutting edges [17]. Authors [16] investigated the microstructure modification of 2024 aluminum alloy produced by friction drilling. They showed that the physical processes and the final structure are the same as friction stir welding terminology. They found three zones in the cross-section of the hole section: stir zone (SZ), thermo-mechanically affected zone (TMAZ), and heat affected zone (HAZ). Friction drilling leads to material hardening near the hole with the microhardness monotonically decreasing closer to the base metal (BM). The maximum microhardness was detected in recrystallized material layers in the SZ and it was equal to 1.3 GPa.

Another new method, selective laser melting and direct laser deposition, were investigated [18,19] with Al-6.2Mg-0.36Sc-0.09Zr and Al-4.6Mg-0.66Sc-0.42Zr-0.49Mn aluminum alloys. It was concluded that the highest tensile strengths of 500 MPa and 390 MPa, respectively, can be reached in the alloys using additive methods due to the formation of the fine structure and $\text{Al}_3(\text{Sc,Zr})$ dispersoids. However, a great deal of hot cracking was observed. To obtaining defect-free bulk details by additive manufacturing it is important to predict the behavior of the material during melting as described in [20].

The new heat-treatable, weldable, cryogenic 1545 K (Al-4.7Mg-0.32Mn-0.21Sc-0.1Zr alloy) alloy based on an Al-Mg-Sc system is a very promising material for the aerospace industry [18–24]. The aim of this research was to increase the tensile strength of the laser welded Al-4.7Mg-0.32Mn-0.21Sc-0.1Zr alloy at the expense of the formation of the fine grain structure of the weld.

2. Materials and Methods

The material used in this work was the alloy of grade 1545 K with the chemical composition presented in Table 1.

Table 1. Chemical composition of the investigated alloy 1545 K, mass %.

Al	Mg	Mn	Sc	Zr	Cu	Fe	Zn
bal.	4.7	0.32	0.21	0.1	<0.1	<0.1	<0.1

From a 280-mm-thick industrial ingot, sheets with thicknesses of 10 mm were obtained. The 10-mm sheets were rolled to a thickness of 1 mm using a laboratory rolling mill.

The technology used in [23] involved hot rolling from 28 to 10 mm at 370 °C and cold rolling from 10 to 1 mm.

The laser welding process of thin sheets was carried out on pulse-periodic laser welding machine MUL-1-M-200 (OOO Latikom, Moscow, Russia) equipped with an Nd:YAG laser which operates at a wavelength of 1064 nm. In the present work, the laser power was 200 W, the pulse repetition frequency ranged from 0.5 to 20 Hz; the speed of movement of the stage changed from 0.25 to 20 mm/s; and the

shielding gas was argon. All samples were prepared before welding by electropolishing edge sides using an electrolyte ($C_2H_5OH + HClO_4$) under 20 V and drying in furnace at 150 °C for 10 min.

Samples were annealed after the welding process in a Nabertherm (Nabertherm, Lilienthal, Germany) electric furnace. After welding the welded parts were cut to the standard tensile test specimens using wire electrodischarge machining as an alternative process to milling due to the possibility to produce specimens which easily meet the geometric-dimensional requirements, no affectation to the ductility of the edge and, finally, the lack of any significant change in the mechanical properties [25].

Samples were polished with Struers Labopol-5 (Struers-Ensuring Certainty, Ballerup, Denmark) equipment for the microstructural and microhardness investigations. The grain structure was analyzed after the oxidation reaction of the polished surface with 10% electrolyte (saturated solution H_3BO_3 in HF) in distilled water at 17 V.

The polished samples were observed under polarized light using a Neophot-30 (Carl Zeiss Jena, Oberkochen, Germany) optical microscope. The microstructure, phase composition, and distribution of elements in the weld were investigated by using a TESCAN VEGA 3LMH (Tescan, Kohoutovice, Česká Republika) scanning electron microscope (SEM).

The small polished and etched samples were tested with an HVD-1000AP micro Vickers (Germany Wolpert Wilson Instruments, Aachen, Germany,) hardness testing machine with a hardness scale of HV0.2, a time duration of 5 s, and a test force of 1960 N, with the shape of the indenter being a square-based diamond pyramid with an apical angle of 136°. The tensile tests were performed using a Zwick/Roell Z250 (Zwick/Roell, Kennesaw, GA, USA) Allround series-testing machine. The strain rate was 4 mm per minute. The standard deviation from the mean value was within $\pm(2-4)$ MPa of the measured value. A new overview about the innovative testing machine and methodology are presented in [26,27].

3. Results and Discussion

3.1. Laser Welding Parameters

The production of a good quality weld depends on the power of the pulse and its duration, the frequency of pulses, and welding rate, the determination of the degree of overlap of the single welds formed by individual pulses of a laser beam, as well as the size of the area of a focused beam (active area), and the shape of pulse. The main criteria for power of the pulse, duration, and frequency (which depend on the welding rate and overlap) were the volume of the molten area and splashes. If power, pulse duration, and frequency increases, the molten area and possibility of splashes increases, as well. Thus, the optimal parameters of pulsed laser welding of the Al-4.7Mg-0.32Mn-0.21Sc-0.1Zr alloy were determined by experimental investigation: 330–340 V in voltage, 0.2–0.25 mm in pulse overlap with 12 ms duration, and 2 mm/s in the welding rate. The frequency was 8–10 Hz. The melting zone was 0.6 mm in thickness without strong splashes of metal from the welding zone and the formation of a large steam and gas channel, which leads to the formation of large gas pores at the root of the seam at optimal parameters. A duplex as-cast structure was formed in the welded seam of the investigated alloy (butt welding of deformed 1 mm thickness sheets), which consisted of columnar crystals zone and equiaxed crystal zones in the center of the weld (Figure 1).

The formation of the columnar grains had a negative effect on the mechanical properties. A non-homogenous grain structure leads to a decrease in strength and plasticity. Columnar grains are the effective centers for nucleation and propagation of failure cracks.

The main problem of the laser welding of the Al-4.7Mg-0.32Mn-0.21Sc-0.1Zr alloy was high hot cracking susceptibility, which depended of the high effective solidification range and cooling rate during welding. The cooling rate during welding is depends of pulse shape [28–31]. Rectangular and ramp-down pulse shapes were investigated for decreasing the cooling rate (Figure 2). In the first case a constant laser power applied during welding. The temperature gradient between the melt and base metal is greatest. The formation of a long hot crack (Figure 2a) was the result. In the

second case, the pulse shape starts with a constant laser power for 4 ms to generate the required weld pool. After this welding duration, the laser power is linearly decreased during a cooling duration to achieve moderate cooling rates during solidification. Decreasing the laser power led to a decline in hot cracking susceptibility (Figure 2b). The same results were obtained by Michaud et al. [32,33] on different aluminum-copper alloys and by Zhang et al. [31] to weld 6061 aluminum alloys using a ramp-down laser pulse shape.

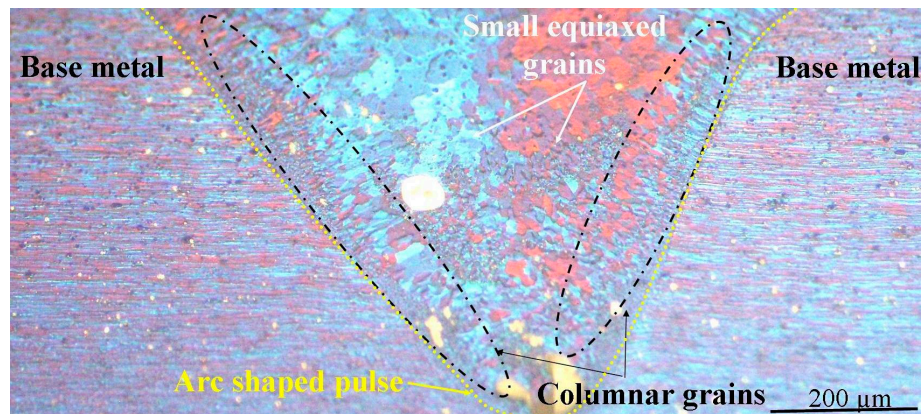


Figure 1. As-cast structure of the welded seam of the Al-4.7Mg-0.32Mn-0.21Sc-0.1Zr alloy.

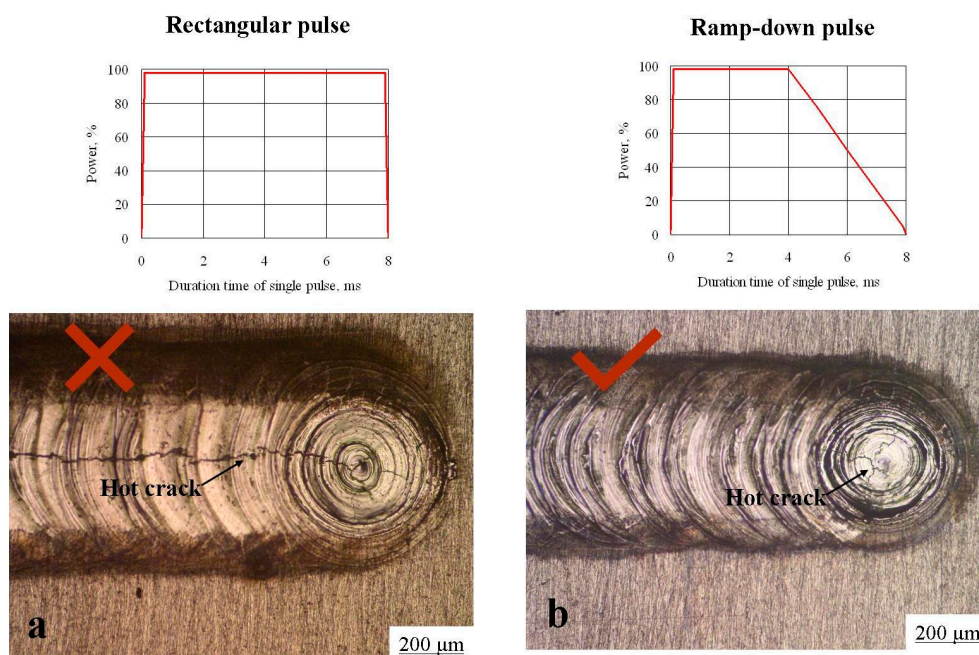


Figure 2. The effect of rectangular (a) and ramp-down (b) pulse shaping on hot cracking.

The results showed that it was possible to eliminate solidification cracking in 1545 K pulsed Nd:YAG laser welds by decreasing the temperature gradient of the laser pulse power after the main welding pulse sector; thus, the temperature difference between the molten pool and room temperature decreases and the speed of cooling rate decreases, as well, and the hot cracking will decrease or disappear.

3.2. Influence of Filler Metal on Weldability

Two filler materials were used for pulse laser welding of the Al-4.7Mg-0.32Mn-0.21Sc-0.1Zr alloy. Al-5Mg (AlMg) alloy and Al-5Ti-1B (AlTiB) master alloy were used as a filler metal. Al-5Mg (AlMg) alloy often used filler metal in argon arc welding of Al-Mg alloys. Al-5Ti-1B (AlTiB) master alloy is an effective grain refiner. Al_3Ti are the primary crystals which form during solidification and the TiB_2 phase is the effective grain refiner. This phase has similar lattice parameters ($a = 0.5446$ nm and $a = 0.3029$ nm for Al_3Ti and TiB_2 , respectively) with Al ($a = 0.4049$ nm). The filler material 0.25 mm in thickness was placed between two sheets of the base alloy. Figure 2 demonstrates the microstructure of the laser-welded alloy with metals.

Columnar crystal zones and equiaxed crystal zones in the center of the weld were found after welding without and with AlMg filler metal. Hot cracks and gas porosity appeared as defects in the weld. The fine grain structure with an average grain size in 4 ± 0.2 μm was formed in the weld zone after using AlTiB filler metal. Significant grain refinement led to increasing hot cracking susceptibility [7,34]. Figure 3 illustrated microstructure and distribution of the alloying elements in the weld of the Al-4.7Mg-0.32Mn-0.21Sc-0.1Zr alloy after welding with AlTiB. High density of the TiB_2 phase was found in the weld. Zr and Sc homogeneously distributed in the solid solution. Figure 4 illustrates the distribution of the elements in the base metal and welding zone. The mixture of the base and filler metals was formed during laser welding with an average concentration of Mg, 2.8%; Mn, 0.2%; Zr, 0.1%; Sc, 0.15%; and Ti, 2.1%.

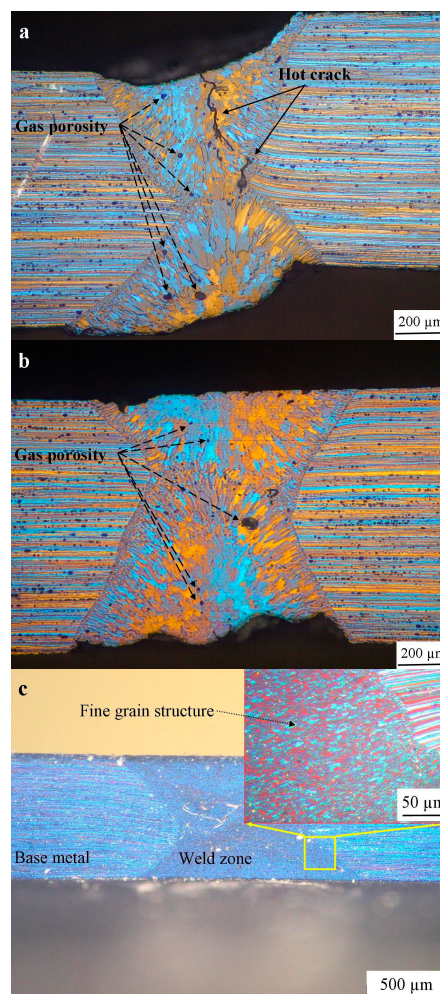


Figure 2. Microstructure of the welded alloy: (a) without filler metal; (b) with AlMg; and (c) with AlTiB filler metals.

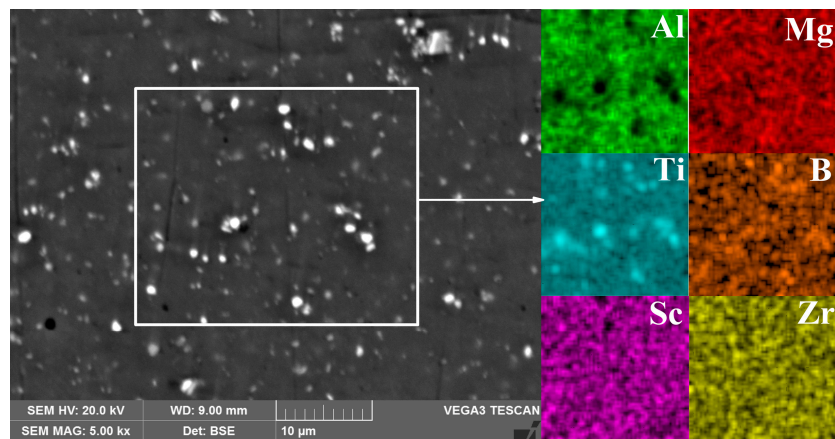


Figure 3. SEM microstructure and distribution of the alloying elements in the weld of the Al-4.7Mg-0.32Mn-0.21Sc-0.1Zr alloy after welding with AlTiB.

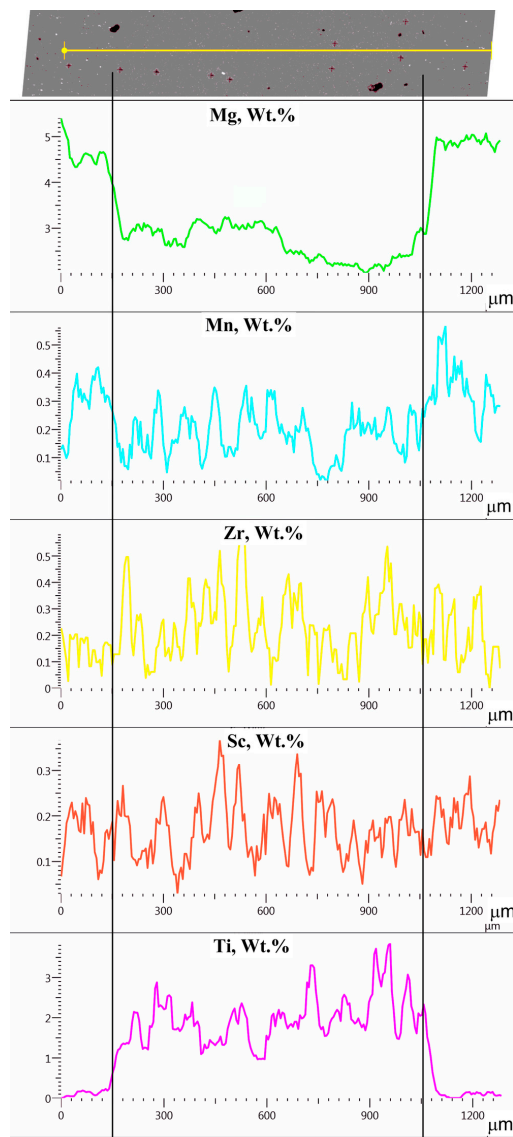


Figure 4. Distribution of the elements in the base metal (outside the lines) and the welding zone (inside the lines) in the Al-4.7Mg-0.32Mn-0.21Sc-0.1Zr alloy after welding with AlTiB.

3.3. Effect of Heat Treatment of Butt-Welded 1545 K Aluminum Alloy

The microhardness of the based Al-4.7Mg-0.32Mn-0.21Sc-0.1Zr alloy and welding zone after welding with AlTiB and annealed at 370 °C for 6 h conditions are presented in Figure 5. The microhardness of the base alloy is 150 μ HV. The transition to the weld microhardness leads to a decrease to 98 μ HV. After annealing at 370 °C for 6 h the softening effect was 30 μ HV for the base metal. The mechanisms of softening were investigated by authors in previous works [22,23]. Hardness increased to 142 μ HV for the weld. The hardening effect of 44 μ HV was achieved through the formation of the Al₃(Sc,Zr) dispersoids.

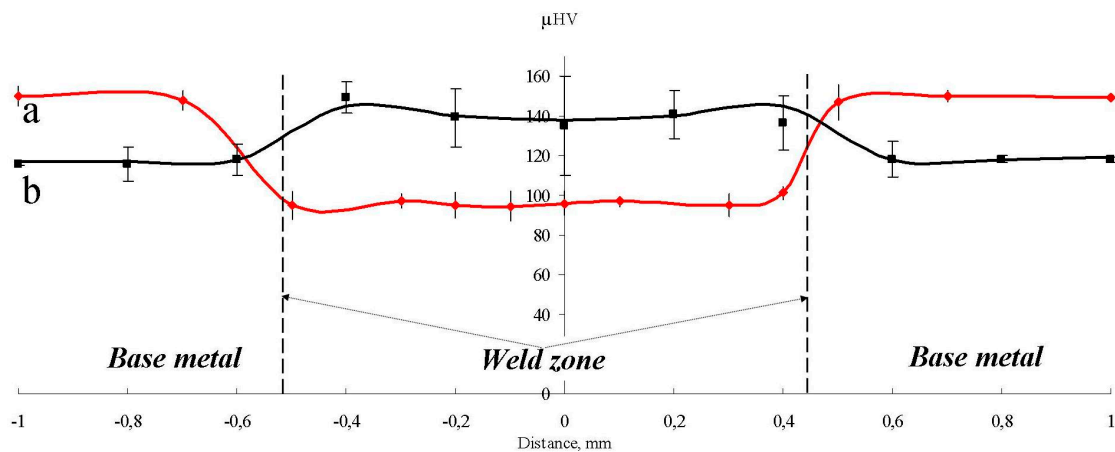


Figure 5. Microhardness over the cross-section of weld zone: (a) 1545 K welded with AlTiB; and (b) 1545 K welded with AlTiB and annealed at 370 °C 6 h.

The UTS of the base and welded Al-4.7Mg-0.32Mn-0.21Sc-0.1Zr alloy in the different conditions are presented in Table 2. The UTS of the welded alloy without filler metal and with the AlMg was 100 MPa. Very low UTS associated with the presence of the hot cracks and porosity in the weld (Figure 2a,b). The UTS after welding with AlTiB was significantly higher—260 MPa. The same strength was for based alloy in the as cast condition. The UTS was increased by 60 MPa after annealing at 370 °C for 6 h and it was 85% from UTS of the base alloy at the same condition.

Table 2. UTS of the investigated alloy under the different conditions.

Condition	UTS, MPa
As cast	268 ± 8
As cast and annealed at 370 °C for 6 h	360 ± 10
As cast, annealed and rolled	490 ± 12
Rolled and annealed at 370 °C for 6 h	375 ± 8
Welded without filler metal	100 ± 9
Welded with AlMg	90 ± 7
Welded with AlTiB	260 ± 7
Welded with AlTiB and annealed at 370 °C for 6 h	320 ± 8

4. Conclusions

Al-Mg alloys are the weldable aluminum alloys. However, they have high hot cracking susceptibility during argon-arc welding and high gas porosity after gas welding. The present article showed that pulsed laser welding is one the new methods of joining that reduces the hot cracking and gas porosity formation and increases the mechanical properties of the weld zone in aluminum alloys. It was concluded that:

1. The optimal parameters of pulsed laser welding of the Al-4.7Mg-0.32Mn-0.21Sc-0.1Zr alloy were determined. They were 330–340 V in voltage, 0.2–0.25 mm in pulse overlap with 12 ms duration, and 2 mm/s in welding speed with a ramp-down pulse shape.
2. It was found that pulsed laser welding of the alloy without and with AlMg filler metal led to the formation of a duplex as-cast structure with hot cracks and gas porosity as defects in the weld zone. The fine grain structure with an average grain size of $4 \pm 0.2 \mu\text{m}$ and without any weld defects was formed in the weld zone after using AlTiB filler metal.
3. The mixture of the base and filler metals was formed during laser welding with average concentrations of Mg, 2.8%; Mn, 0.2%; Zr, 0.1%; Sc, 0.15%; and Ti, 2.1%. The high density of the TiB₂ phase was found in the weld. Zr and Sc were homogeneously distributed in the solid solution.
4. The UTS of the Al-4.7Mg-0.32Mn-0.21Sc-0.1Zr alloy welded with AlTiB was 320 MPa after annealing at 370 °C for 6 h and it was 85% of the UTS of the base alloy at the same condition.

Author Contributions: Irina Loginova performed most of the experiments and wrote the manuscript. Asmaa Khalil helped with preparation of experimental equipment and specimens for laser welding, tensile tests, and microstructure investigation. Andrey Pozdnyakov helped to analyze the experimental data and gave some constructive suggestions. Alexey Solonin helped with some experiments and discussion of the results. Vadim Zolotarevsky participated in the results discussion and guided the writing of the article.

Conflicts of Interest: The authors declare no conflict of interest.

References

1. Lathabai, S.; Lloyd, P.G. The effect of scandium on the microstructure, mechanical properties and weldability of a cast Al–Mg alloy. *Acta Mater.* **2002**, *50*, 4275–4292. [[CrossRef](#)]
2. Filatov, Y.A.; Yelagin, V.I.; Zakharov, V.V. New Al–Mg–Sc alloys. *Mater. Sci. Eng. A* **2000**, *280*, 97–101. [[CrossRef](#)]
3. Tao, Y.; Zhang, Z.; Ni, D.R.; Wang, D.; Xiao, B.L.; Ma, Z.Y. Influence of welding parameter on mechanical properties and fracture behavior of friction stir welded Al–Mg–Sc joints. *Mater. Sci. Eng. A* **2014**, *612*, 236–245. [[CrossRef](#)]
4. Leo, P.; Renna, G.; Casalino, G.; Olabi, A.G. Effect of power distribution on the weld quality during hybrid laser welding of an Al–Mg alloy. *Opt. Laser Technol.* **2015**, *73*, 118–126. [[CrossRef](#)]
5. Kuo, T.Y.; Lin, H.C. Effects of pulse level of Nd–YAG laser on tensile properties and formability of laser weldments in automotive aluminum alloys. *Mater. Sci. Eng. A* **2006**, *416*, 281–289. [[CrossRef](#)]
6. Novikov, I.I. *Goryachelomkost Tsvetnykh Metallov i Splavov (Hot Shortness of Non-Ferrous Metals and Alloys)*; Nauka: Moscow, Russia, 1966; p. 300.
7. Eskin, D.G.; Suyitno; Kargerman, L. Mechanical properties in the semi-solid state and hot tearing of aluminium alloys. *Prog. Mater. Sci.* **2004**, *49*, 629–711. [[CrossRef](#)]
8. Zolotarevskiy, V.S.; Pozdnyakov, A.V.; Khvan, A.V. Thermodynamic calculations of the effective solidification range and its relation to hot cracking of aluminum-based ternary alloys. *Russ. J. Non-Ferrous Met.* **2011**, *52*, 50–55. [[CrossRef](#)]
9. Lashko, N.F.; Lashko-Avakyan, S.V. *Svarivoyaymie Legkie Splavy (Light-Weight Welded Alloys)*; Petrov, G.L., Ed.; Subpromgiz: St.-Petersburg, Russia, 1960; pp. 194–229.
10. Argade, G.R.; Kumar, N.; Mishra, R.S. Stress corrosion cracking susceptibility of ultrafine grained Al–Mg–Sc alloy. *Mater. Sci. Eng. A* **2013**, *565*, 80–89. [[CrossRef](#)]
11. Besel, Y.; Besel, M.; Alfaro, U.M.; Kakiuchi, T.; Hirata, T.; Uematsu, Y. Influence of local fatigue damage evolution on crack initiation behavior in a friction stir welded Al–Mg–Sc alloy. *Int. J. Fatigue* **2017**, *99*, 151–162. [[CrossRef](#)]
12. Yang, D.; Li, X.; He, D.; Huang, H. Effect of minor Er and Zr on microstructure and mechanical properties of Al–Mg–Mn alloy (5083) welded joints. *Mater. Sci. Eng. A* **2013**, *561*, 226–231. [[CrossRef](#)]
13. Fu, L.; Peng, Y.; Huang, J.; Deng, Y.; Yin, Z. Microstructures and mechanical properties of Gas Tungsten Arc Welded joints of new Al–Mg–Sc and Al–Mg–Er alloy plates. *Mater. Sci. Eng. A* **2015**, *620*, 149–154. [[CrossRef](#)]
14. Urbikain, G.; Perez, J.M.; de Lacalle, L.N.L.; Andueza, A. Combination of friction drilling and form tapping processes on dissimilar materials for making nutless joints. *Proc. Inst. Mech. Eng. B J. Eng. Manuf.* **2016**. [[CrossRef](#)]

15. Boopathi, M.; Shankar, S.; Manikandakumar, S.; Ramesh, R. Experimental investigation of friction drilling on brass, aluminium and stainless steel. *Procedia Eng.* **2013**, *64*, 1219–1226. [[CrossRef](#)]
16. Eliseev, A.A.; Fortuna, S.V.; Kolubaev, E.A.; Kalashnikova, T.A. Microstructure modification of 2024 aluminum alloy produced by friction drilling. *Mater. Sci. Eng. A* **2017**, *691*, 121–125. [[CrossRef](#)]
17. De Lacalle, L.N.L.; Urbikain, G.; Azkona, I.; Zumalde, E.; Okariz, L. Friction drilling, form tapping and rotary broaching for fast joining technologies. *Weld. Mater. Test.* **2016**, *4*, 3–7.
18. Spierings, A.B.; Dawson, K.; Kern, K.; Palm, F.; Wegener, K. SLM-processed Sc- and Zr-modified Al-Mg alloy: Mechanical properties and microstructural effects of heat treatment. *Mater. Sci. Eng. A* **2017**, *701*, 264–273. [[CrossRef](#)]
19. Li, R.; Wang, M.; Yuan, T.; Song, B.; Chen, C.; Zhou, K.; Cao, P. Selective laser melting of a novel Sc and Zr modified Al-6.2 Mg alloy: Processing, microstructure, and properties. *Powder Technol.* **2017**, *319*, 117–128. [[CrossRef](#)]
20. Taberero, I.; Lamikiz, A.; Martínez, S.; Ukar, E.; de Lacalle, L.N.L. Modelling of energy attenuation due to powder flow-laser beam interaction during laser cladding process. *J. Mater. Process. Technol.* **2012**, *212*, 516–522. [[CrossRef](#)]
21. Zhen, H.; Yong, P.; Zhi, Y.; Xue, L. Comparison of FSW and TIG welded joints in Al-Mg-Mn-Sc-Zr alloy plates. *Trans. Nonferrous Met. Soc. China* **2011**, *21*, 1685–1691. [[CrossRef](#)]
22. Zolotarevskiy, V.S.; Dobrozinskaya, R.I.; Cheverikin, V.V.; Khamnagdaeva, E.A.; Pozdniakov, A.V.; Levchenko, V.S.; Besogonova, E.S. Strength and substructure of Al-4.7Mg-0.32Mn-0.21Sc-0.09Zr alloy sheets. *Phys. Met. Metallogr.* **2017**, *118*, 407–414. [[CrossRef](#)]
23. Zolotarevskiy, V.S.; Dobrojinskaja, R.I.; Cheverikin, V.V.; Khamnagdaeva, E.A.; Pozdniakov, A.V.; Levchenko, V.S.; Besogonova, E.S. Evolution of the structure and mechanical properties of sheets of the of Al-4.7Mg-0.32Mn-0.21Sc-0.09Zr alloy due to deformation accumulated upon rolling. *Phys. Met. Metallogr.* **2016**, *117*, 1163–1169. [[CrossRef](#)]
24. Filatov, Y.A.; Baidin, G.G.; Dobrozinskaya, R.I.; Khamnagdaeva, E.A.; Ovsyannikov, B.V. A new 1545K Al-Mg-Sc system-based heat-treatable weldable cryogenic alloy. *Tekhnol. Legk. Splavov.* **2014**, *1*, 32–36.
25. Martínez Krahmer, D.; Polvorosa, R.; de Lacalle, L.N.L.; Alonso-Pinillos, U.; Abate, G.; Riu, F. Alternatives for specimen manufacturing in tensile testing of steel plates. *Exp. Tech.* **2016**, *40*, 1555–1565. [[CrossRef](#)]
26. Silva, C.M.A.; Rosa, P.A.R.; Martins, P.A.F. Innovative testing machines and methodologies for the mechanical characterization of materials. *Exp. Tech.* **2016**, *40*, 569–581. [[CrossRef](#)]
27. Dixit, U.S.; Joshi, S.N.; Davim, J.P. Incorporation of material behavior in modeling of metal forming and machining processes: A review. *Mater. Des.* **2011**, *32*, 3655–3670. [[CrossRef](#)]
28. Witzendorff, P.; Kaieler, S.; Suttman, O.; Overmeyer, L. Using pulse shaping to control temporal strain development and solidification cracking in pulsed laser welding of 6082 aluminum alloys. *J. Mater. Process. Technol.* **2015**, *225*, 162–169. [[CrossRef](#)]
29. Dworak, J. *Impact of Laser Beam Shape on YAG Pulsed Laser Welding*; Biuletyn Instytutu Spawalnictwa: Gliwice, Poland, 2012; pp. 5–14.
30. Lienert, T.J.; Lippold, J.C. Improved weldability diagram for pulsed laser welded austenitic stainless steel. *Sci. Technol. Weld. Join.* **2003**, *8*, 1–9. [[CrossRef](#)]
31. Zhang, J.; Weckmann, D.C.; Zhou, Y. Effects of temporal pulse shaping on cracking susceptibility of 6061-T6 aluminum Nd:YAG laser welds. *Weld. J.* **2008**, *87*, 18–30. [[CrossRef](#)]
32. Michaud, E.J.; Kerr, H.W.; Weckman, D.C. Temporal Pulse Shaping and Solidification Cracking in Laser Welded Al-Cu Alloys. In Proceedings of the 4th International Conference on Trends in Welding Research, Gatlinburg, TN, USA, 5–8 June 1995; pp. 153–158.
33. Michaud, E.J.; Weckmann, D.C.; Kerr, H.W. Effect of Pulse Shape on Predicted Thermomechanical Strains in Nd:YAG Laser Welded Aluminum. In Proceedings of the International Congress on Applications of Lasers and Electro Optics, Orlando, FL, USA, 1994; pp. 461–470.
34. Eskin, D.G.; Katgerman, L.; Suyitno; Mooney, J.F. Contraction of aluminum alloys during and after solidification. *Metall. Mater. Trans. A* **2004**, *35*, 1325–1335. [[CrossRef](#)]

